

Chapter 2

Modeling Microbolometer Performance

Since the dynamics of microbolometer operation involve components of current flow as well as heat flow, both circuit analysis and thermal modeling must be integrated in order to model actual microbolometer performance. By developing such models, the electrical and thermal responses can be related to material properties and device geometry. An understanding of these relationships is essential in making material and geometric choices for these devices.

2.1 Analytical Models of Thermal Impedances

2.1.1 Heat Flow Paths

Simplified thermal models which can be solved analytically can be used as tools to model bolometer operation. While simplified models may not provide exact thermal information, they can provide an easy method to approximate the effects of scaling and material properties on device performance. They can also be used to compare the influence of different mechanisms of heat flow out of the detector.

Figure 2.1 illustrates a model which separates the heat flow out of a microbolometer into three distinct mechanisms. The responsivity model treats the detector as a lumped element, by approximating the detector as a small region of constant temperature. In a real microbolometer, the temperature will vary throughout the detector. Z_d represents the thermal impedance for the heat leaving the ends of the detector directly into the electrical leads of the antenna. In this model, the antenna leads are approximated as perfect heat sinks, and therefore remain at the ambient temperature. Z_{sub} is the impedance for the heat which leaves the system through the substrate. Z_{fringe} corresponds to heat which enters the substrate and is then coupled into the antenna leads.

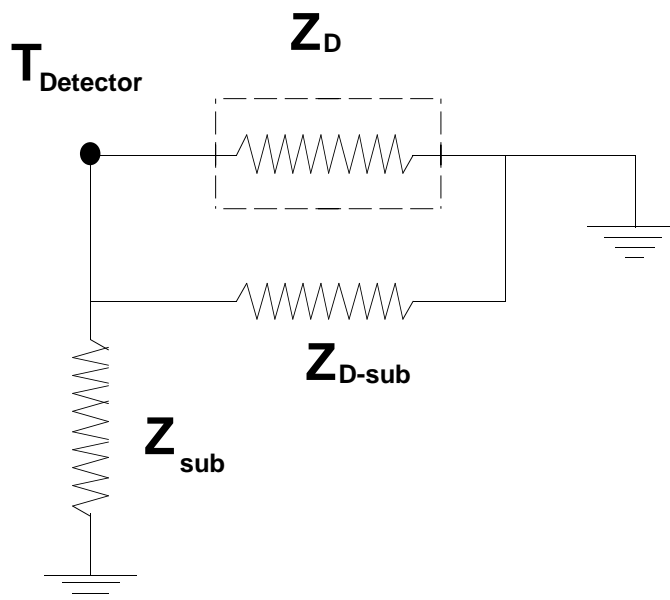


Figure 2.1 Heat flow paths for heat leaving an antenna-coupled microbolometer.

2.1.2 Heat Conduction Directly Through the Antenna Leads

The thermal solution for the impedance for heat flow through the ends of the heater directly into the leads can be estimated by approximating the leads as perfect heat sinks. By assuming that heat is generated uniformly within the detector, and that the ends are attached to perfect heat sinks, the temperature profile can be solved as equation 2.1

$$T(x) = \frac{q' \cdot L^2}{2 \cdot k} \cdot \left(\frac{x}{L} - \left(\frac{x}{L} \right)^2 \right) \quad (2.1)$$

where L is the length of the bar, and q' is density of heat generation within bar. The profile for this solution is shown in figure 2.2, where T_{max} is calculated as

$$T_{\max} = \frac{q' \cdot L}{8 \cdot k} \quad (2.2)$$

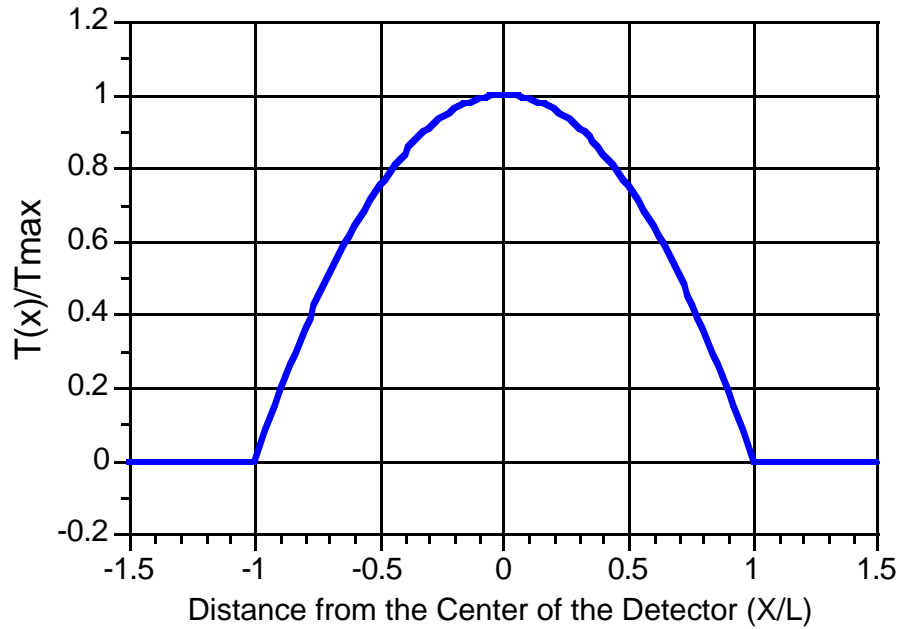


Figure 2.2 Thermal profile for a microbolometer without a substrate. The profile shown here considers only heat flow directly into the antenna leads.

A value for effective thermal impedance can be obtained by dividing the average temperature by the total power dissipated within the bar. The result is shown in equation 2.3 below.

$$Z_d = \frac{L}{12 \cdot k \cdot t \cdot w} \quad (2.3)$$

The dimensions of the detector must be chosen so that its resistance matches the embedding impedance of the antenna structure. By calculating the detector resistance as

$$R = \frac{\rho \cdot L}{w \cdot t} \quad (2.4)$$

the steady state thermal impedance of the detector can be expressed as

$$Z_d = \frac{R}{12} \cdot \frac{\sigma}{k} \quad (2.5)$$

It has been pointed out by Neikirk [1] that for a fixed device resistance, almost all metals would result in nearly the same thermal impedance out the leads. This is because the ratio of electrical conductivity to thermal conductivity metals is strongly guided by the Wiedmann-Franz law, stated as

$$\frac{\sigma}{k} = \frac{3}{\pi^2} \cdot \left(\frac{e}{k_B} \right)^2 \cdot \frac{1}{T} \quad (2.6)$$

where e is the electron charge, k_B is the Boltzmann constant, and T is the absolute temperature. Table 2.1 lists several metals and their respective electrical and thermal conductivities as well as the temperature coefficient of conductivity.

Bismuth films are somewhat troublesome to model because the thin film properties can be very different from bulk properties, and are sensitive to deposition conditions. Reports on the electrical properties of bismuth films are given by Wentworth [2], Neikirk [1], and Abrosimov et al[3]. The resistivity generally increases with decreasing film thickness and is somewhat predictable. There have been fewer studies which have reported thermal conductivity values for these films. Although the reported values show a trend of increased thermal conductivity with increased electrical conductivity, the ratio of these values varied considerably (see table 2.1). The film which had a high resistivity[4] had a significantly lower σ/k ratio than those reported which had lower resistivities[3], although this apparent difference may possibly be due to different experimental procedures.

Material	Thermal Conductivity k (W/cm/K)	Electrical Resistivity ρ ($\mu\Omega$ -cm)	σ/k (K/ Ω /W)	Temperature Coefficient of Resistance (K ⁻¹)
Bi (bulk)	0.0792 ²	~ 120 ²	1.1 x 10 ⁵	0.003 ²
Bi (thin film) 1000 Å	~0.029 ³	~ 875 ³	3.9 x 10 ⁴	-
Bi (thin film) 1000 Å	~0.015 ⁶	~ 300 ⁶	2.2 x 10 ⁵	-
Bi (thin film) 3000 Å	~0.033 ⁶	~ 140 ⁶	2.2 x 10 ⁵	-
Bi (thin film)	~0.018 ⁵	~750 ⁴	7.5 x 10 ⁴ ⁵	0.003 ⁵
Au	3.15 ¹	2.249 ¹	1.41 x 10 ⁵	0.00367 ¹
Ag	4.26 ¹	1.628 ¹	1.44 x 10 ⁵	0.00373 ¹
Ni	0.904 ¹	7.16 ¹	1.55 x 10 ⁵	0.00555 ¹
Sn	0.665 ¹	13.194 ¹	1.11 x 10 ⁵	0.00255 ¹
Te	~0.1 ²	4.36 x 10 ⁶ ²	2.3	-
88Au-12Ge	0.439 ¹	30 ¹	7.6 x 10 ⁴	-
Nichrome	0.126 ¹	100 ¹	7.9 x 10 ⁴	0.000127 ¹

Table 2.1 Thermal conductivity and electrical resistivity for various metals used in fabricating microelectronics and thermal detectors. The σ/k values are computed from these values.

- 1 Materials Handbook for Hybrid Microelectronics, Artech House, 1988
- 2 CRC Handbook of Chemistry and Physics, 64th edition, CRC Press, 1984-1984.
- 3 As reported by Neikirk for an air-bridge microbolometer [4]
- 4 Typical values measured at UT Austin.
- 5 Values assumed for most thermal simulations in this study.
- 6 As reported by Abrosimov et al [3]

2.1.3 Heat Conduction into the Substrate

For typical bolometer shapes, in which the length (**L**) to width (**W**) ratios are near 1, the heat flow into the substrate can be approximated as flowing radially from a hemisphere of nearly the same surface area as the area of the detector-substrate interface[1]. For thick substrates (substrate thickness \gg detector dimensions), the substrate can be approximated as a semi-infinite solid. The steady state impedance of a hemispherical surface into a substrate is given by

$$Z_{\text{sub}} = \frac{1}{2 \cdot \pi \cdot k_{\text{sub}} \cdot a} \quad (2.7)$$

where k_{sub} is the thermal conductivity of the substrate and a is the radius of the hemispherical surface. This concept is illustrated in figure 2.3.

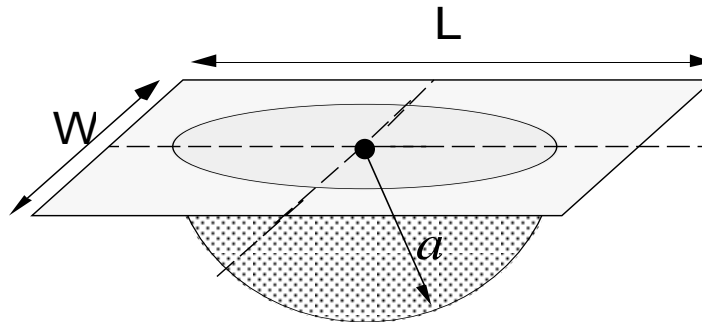


Figure 2.3 Heat flow from a bolometer into a substrate can be modeled as flowing radially from a hemispherical surface. The figure above shows a hemispherical surface of the same area as the square bolometer above it.

To approximate the thermal impedance of a rectangular bolometer on a substrate, the detector-substrate contact area can be approximated as a hemispherical surface of the same area. For this case, the effective radius is

$$a = \sqrt{2 \cdot \pi \cdot L \cdot W} \quad (2.8)$$

By making this assumption, the thermal impedance can be estimated as

$$Z_{\text{sub}} \approx \frac{1}{\sqrt{2\pi} \cdot k_{\text{sub}} \cdot (L \cdot W)^{1/2}} \quad (2.9)$$

Table 2.2 shows the steady state substrate thermal impedance of a square bolometer calculated using the hemispherical approximation as well as by a finite difference method. The results shown here suggest that this approximation is fairly accurate for a square bolometer, but underestimates the impedance by a factor of about 1.2 for a square bolometer.

Area	4 μm^2
Substrate Thermal Conductivity	0.018 W/cm/K
Hemisphere Approximation Z_{sub}	1.1 x 10 ⁵ (K/W)
Finite Difference Z_{sub}	1.3 x 10 ⁵ (K/W)

Table 2.2 Comparing Analytical and Finite difference solutions for thermal impedance into the substrate for a bolometer in which the length and width are equal.

For bolometers with large length-to-width aspect ratios, the heat flow into the substrate becomes more difficult to model analytically. Consider a long, rectangular, isolated bolometer on a semi-infinite substrate with no antenna leads. If the thermal conductivity of the substrate is much lower than the thermal conductivity of the bolometer, then heat flow out of the bolometer will be determined primarily by the temperature profile within the substrate. It can be shown that an infinitely long cylinder embedded into the surface of a semi-infinite solid will have an infinite thermal impedance per unit length. Therefore, the finite bolometer will approach a finite temperature when the temperature profiles into the substrate are roughly spherical. Figure 2.4 shows the normalized thermal impedance as a function of aspect ratio, for bolometers of constant width. The crosses show the impedance calculated using a 3-d finite difference method. The upper line represents the thermal impedance of a square bolometer of the same area as the long bolometer (with a dependence on dimensions as shown in equation 2.9). As expected, the thermal impedance of a long bolometer is lower than the thermal impedance of a square bolometer of the same area. The lower line represents a square bolometer of the same width as the length. We would expect that the impedance of a rectangular bolometer would have a dependence somewhere between $1/\sqrt{L}$ and $1/L$ from the square bolometer value. The middle curve shows a curve fit computed by assuming a $1/L^{0.6}$ dependence on length for a fixed width.

The data in table 2.2 and figure 2.4 gives enough data to create an empirical formula for closely estimating the thermal impedance into the substrate for various aspect ratios. Table 2.2 shows that the hemispherical approximation underestimates the impedance by a factor of about 1.2 for a square bolometer. The data in figure 2.4 shows that the actual impedance has about $1/L^{0.6}$ dependence on length for a fixed width. By combining these two relationships, an empirical formula can be given as

$$Z_{\text{sub}} = 1.2 \cdot \frac{1}{\sqrt{2\pi} \cdot k_{\text{sub}} \cdot (W \cdot L)^{0.5}} \cdot \frac{1}{(L / W)^{0.1}} \quad (2.10)$$

An alternate way of expressing this relation is

$$Z_{\text{sub}} = \frac{1.2}{\sqrt{2\pi} \cdot k_{\text{sub}} \cdot L^{0.6} \cdot W^{0.4}} \quad (2.11)$$

It is unclear whether different substrate thermal conductivities will have a significant effect on the influence of aspect ratios on the thermal impedance.

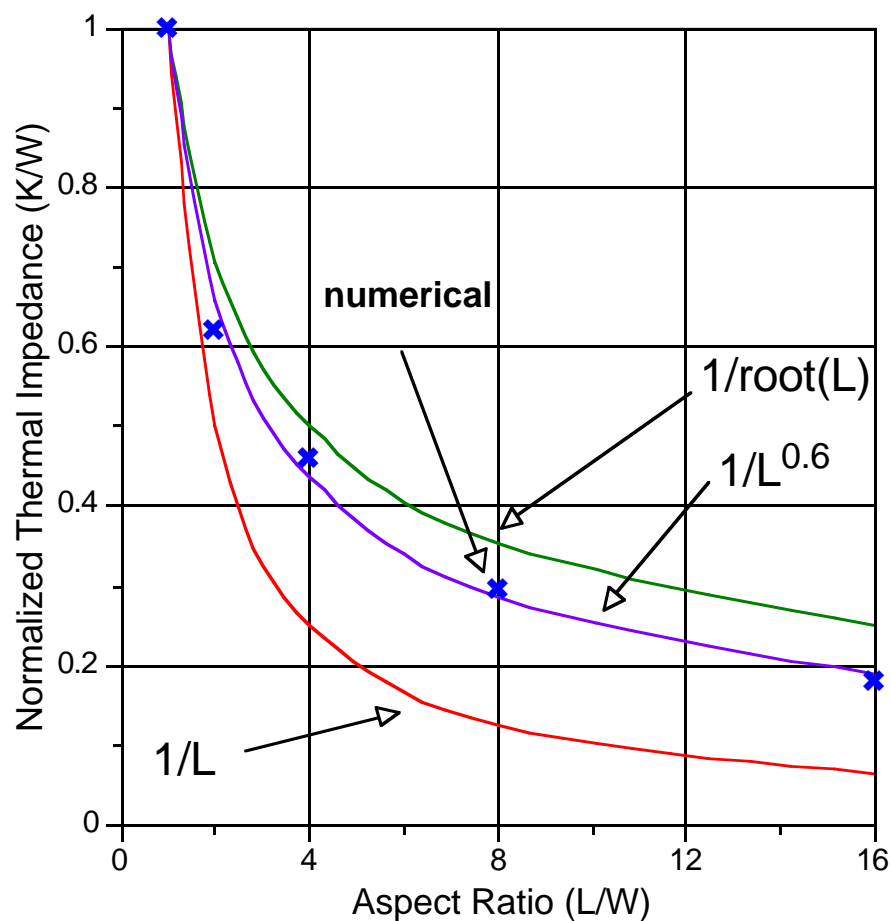


Figure 2.4 Normalized steady state thermal impedance for a rectangle on a semi-infinite solid.

The substrate thermal conductivity for these simulations was 0.014 W/cm/K.

2.1.4 Substrate to Antenna Fringe Thermal Coupling

Another independent component of heat conduction out of a microbolometer is heat that flows from the detector into the substrate, and is then coupled into the antenna leads. This mechanism is illustrated in figure 2.5. The lines shown denote fringe fields of high thermal gradients toward the antenna. Figure 2.6 shows the isotherms of a bismuth microbolometer computed by a finite difference method.

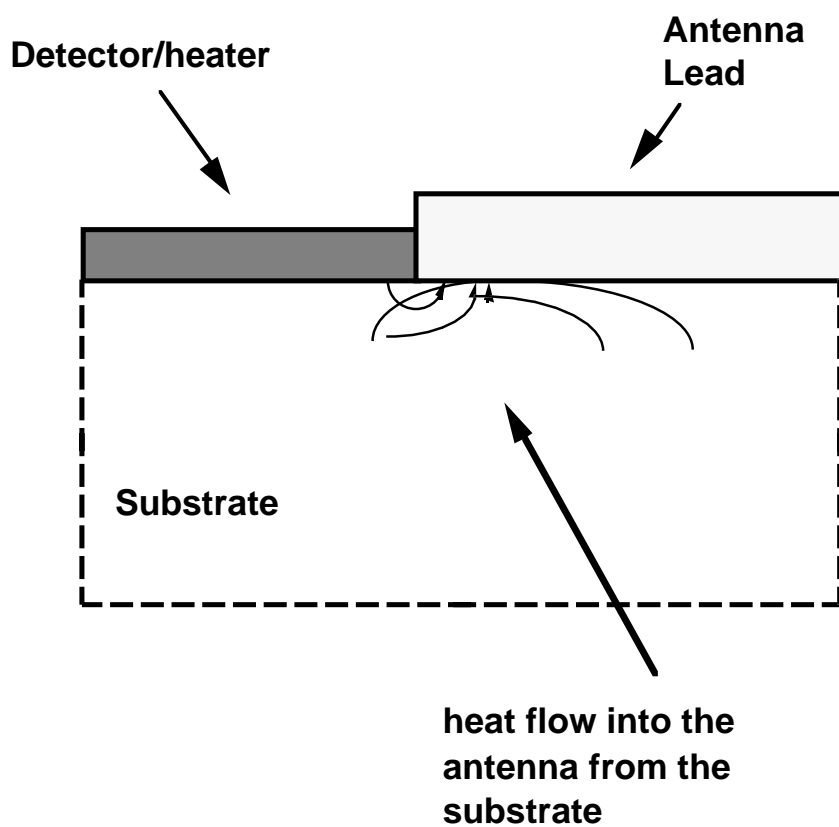


Figure 2.5 Fringe heat conduction from a microbolometer through the substrate and into the antenna leads.

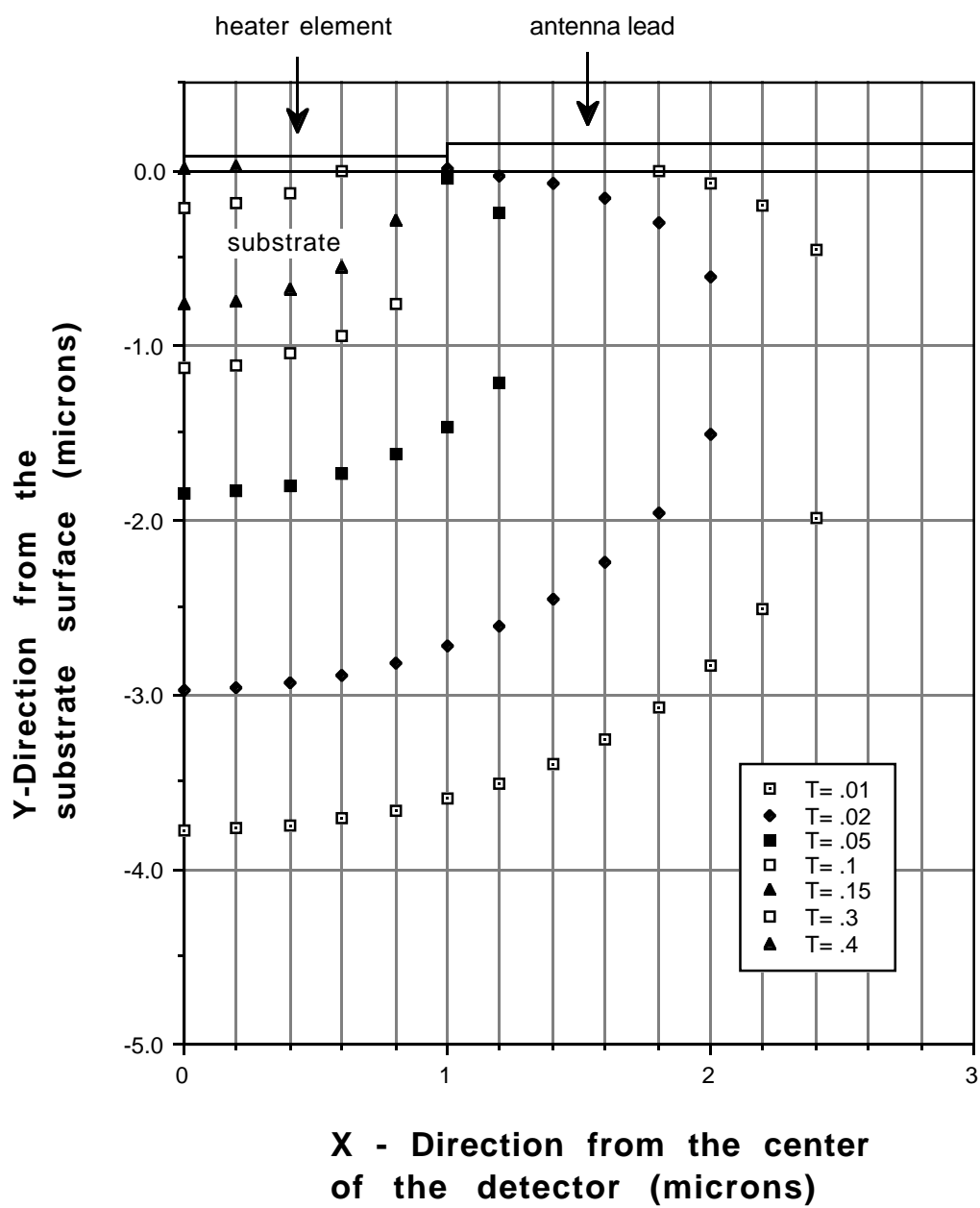


Figure 2.6 Isothermal profiles into the substrate of an antenna-coupled microbolometer

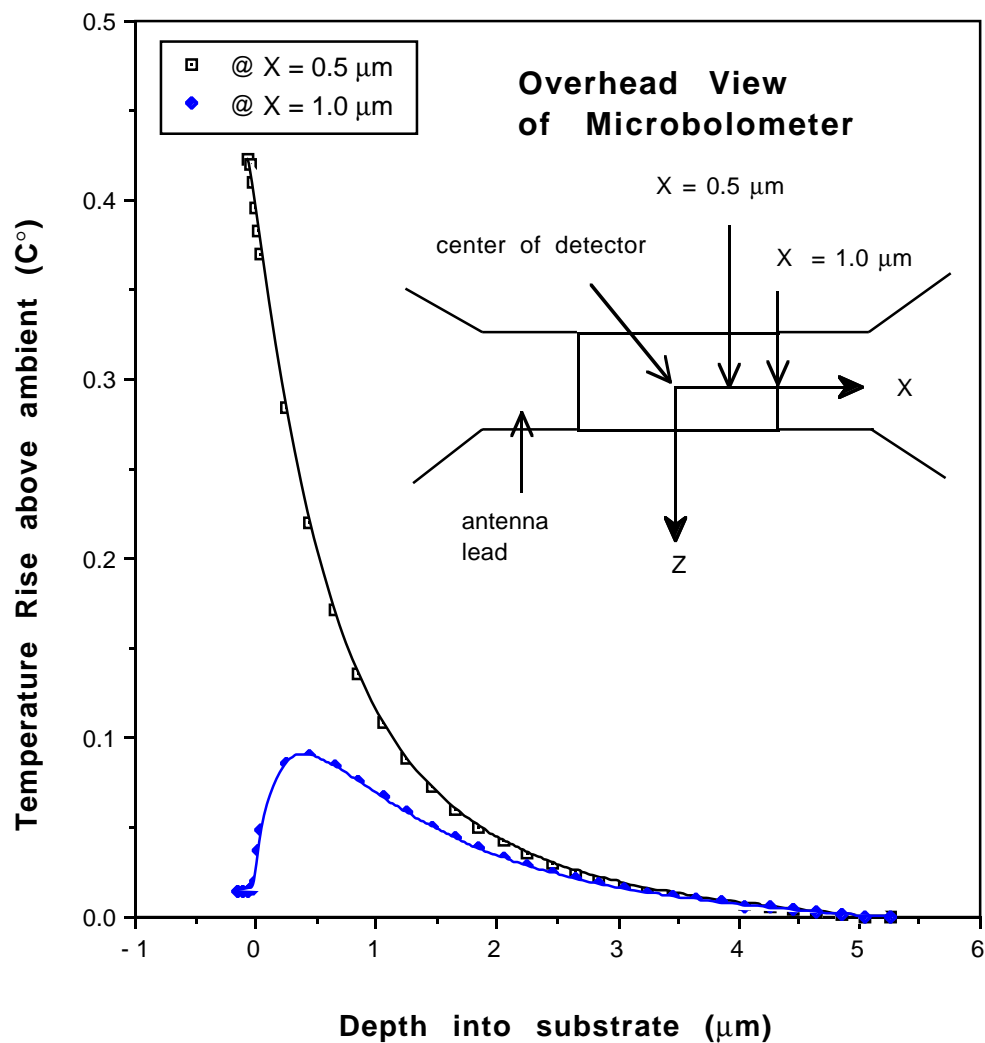


Figure 2.7 Simulated temperature profiles into the substrate at two points below a bismuth microbolometer (length = $4 \mu\text{m}$, width = $2 \mu\text{m}$). The upper points are calculated at $0.5 \mu\text{m}$ from the center of the microbolometer lengthwise (halfway between the center and the antenna leads). The lower points are measured at the point where the antenna touches the detector ($x = 1.0 \mu\text{m}$). Both sets of points are measured at the center of the detector width ($z = 0$).

Figure 2.7 shows one dimensional temperature profiles into the substrate at two points below the bismuth detector element. The lower curve shows a steep negative temperature gradient in the substrate near the metal lead, indicating a significant amount on heat transport into the lead from the substrate.

Since the modes of heat loss are independent, the overall net impedance can be related to these modes as

$$\frac{1}{Z_{\text{net}}} = \frac{1}{Z_{\text{d}}} + \frac{1}{Z_{\text{sub}}} + \frac{1}{Z_{\text{fringe}}} \quad (2.12)$$

By using a finite difference method to solve for Z_{net} , and the empirical formula shown in equation 2.11 to approximate Z_{sub} , the value for heat loss though the fringe mechanism can be calculated as

$$Z_{\text{fringe}} = \left[\frac{1}{Z_{\text{net}}} - \frac{1}{Z_{\text{d}}} - \frac{1}{Z_{\text{sub}}} \right]^{-1} \quad (2.13a)$$

This relation can also be expressed as thermal admittances

$$Y_{\text{fringe}} = Y_{\text{net}} - Y_{\text{d}} - Y_{\text{sub}} \quad (2.13b)$$

Table 2.3 lists the input parameters and the results of impedance calculations for bismuth microbolometers of fixed width with gold antenna leads. These impedance results are also shown in figure 2.8a. Figure 2.8b displays the same results as thermal admittances. In this graph, the net admittance (Y_{net}) can be seen the linear sum of the other components. These admittance values are also proportional to the amount of heat loss through each mechanism. The detector thickness was scaled for constant electrical and thermal impedance to the electrical leads. Values for Z_{net} were found using the finite difference method. Z_{d} was calculated using equation 2.3, and Z_{sub} was calculated using equation 2.11.

detector length	1 μm	2 μm	4 μm	8 μm
detector width	2 μm	2 μm	2 μm	2 μm
detector thickness	375 \AA	750 \AA	1500 \AA	3000 \AA
detector thermal conductivity (W/cm/K) [bismuth]	0.033	0.033	0.033	0.033
substrate thermal conductivity (W/cm/K) [glass]	0.018	0.018	0.018	0.018
antenna thermal conductivity (W/cm/K) [gold]	3.15	3.15	3.15	3.15
Z_{net} (K/W)	7.15×10^4	7.96×10^4	6.8×10^4	5.28×10^4
Z_{d} (K/W)	6.17×10^5	6.17×10^5	6.17×10^5	6.17×10^5
Z_{sub} (K/W)	2.02×10^5	1.33×10^5	8.77×10^4	5.79×10^4
Z_{fringe} (K/W)	1.35×10^5	2.92×10^5	5.93×10^5	2.41×10^7
$Z_{\text{net}}/Z_{\text{d}}$	0.12	0.13	0.11	0.086
$Z_{\text{net}}/Z_{\text{sub}}$	0.35	0.60	0.78	0.91
$Z_{\text{net}}/Z_{\text{fringe}}$	0.53	0.27	0.11	0.0022

Table 2.3 Individual Components of thermal impedance and heat loss for a bismuth microbolometers of fixed width (2 μm) and various lengths.

Z_{fringe} was found with these results using equation 2.13a. The values of $Z_{\text{net}}/Z_{\text{fringe}}$, $Z_{\text{net}}/Z_{\text{sub}}$, and $Z_{\text{net}}/Z_{\text{d}}$ are given to show what fraction of heat loss is due to the fringe, substrate, and detector lead mechanism respectively. The 2 μm detector width chosen for this data represents a typical microbolometer width that can be readily fabricated using contact lithography with a self-aligned photoresist air-bridge lift-off technique (see chapter 4, section 4.5).

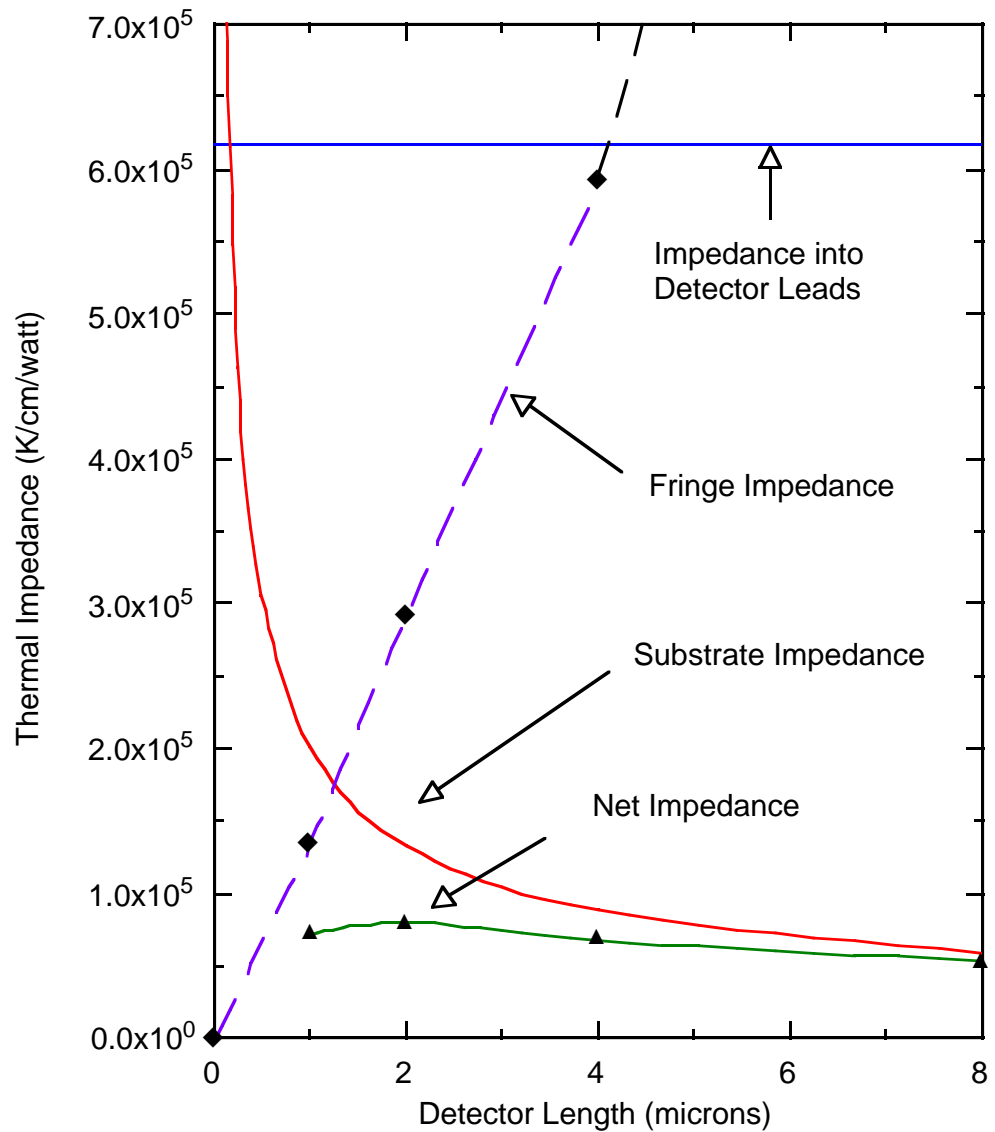


Figure 2.8a Steady state lumped thermal impedance for bismuth microbolometer of various lengths. The bolometer width was fixed at $2 \mu\text{m}$, while the thickness was scaled for constant thermal and electrical impedance to the antenna leads.

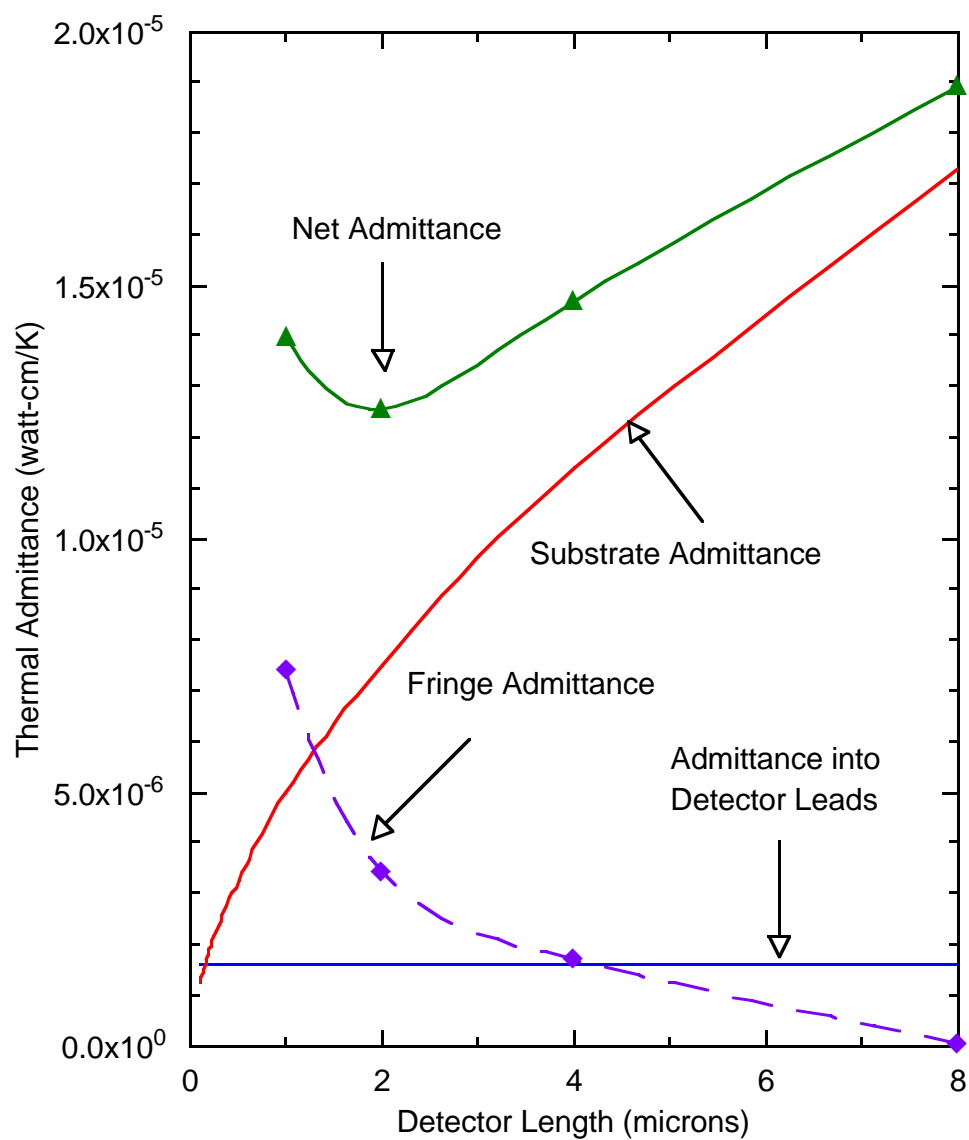


Figure 2.8b Steady state lumped thermal impedance for bismuth microbolometer of various lengths. The bolometer width was fixed at $2 \mu\text{m}$, while the thickness was scaled for constant thermal and electrical impedance to the antenna leads.

The results presented here suggest that the net thermal impedance of the device is relatively insensitive to changes in detector length for lengths greater than about 1 μm , with an optimum detector length for maximum thermal impedance near 2 μm . For long detectors (length $> \sim 4 \mu\text{m}$), heat loss is dominated by heat conduction directly into the substrate, and can accurately be approximated by equation 2.11. For short detectors (length $\leq \sim 1 \mu\text{m}$), heat loss appears to be strongly dominated by the fringe mechanism and increases sharply with decreasing detector length. The impedance curve for the fringe mechanism was extended to zero at length=0 since the fringe impedance would be expected to approach zero as the detector leads are brought together. The curve for the fringe mechanism appears to be linear; at least for short to moderate detector lengths. Due to the nature of these particular calculations, the error in the fringe impedance values will increase as the detector length increases. Fortunately, the influence of the fringe mechanism becomes negligible for this case and will not be important in computing the net thermal impedance.

It should be strongly noted that the curves in figure 2.8a and figure 2.8b are for a specific detector width, substrate thermal conductivity, and detector thermal conductivity. Since the detector thickness was scaled to allow for constant electrical resistance of the detector, the value of \mathbf{Z}_d will be dependent on the resistance chosen, as well as the σ/k ratio of the detector material. Variations in these detector parameters will cause the \mathbf{Z}_d values to shift up or down. For the line width chosen for these curves, however, \mathbf{Z}_d was an insignificant component of the net thermal impedance for all detector lengths. As the line width is reduced, \mathbf{Z}_{sub} would be expected to increase (as described by equation 2.11), while \mathbf{Z}_d would remain constant. Therefore, \mathbf{Z}_d would be expected to become a significant component of heat loss for very small detector widths. The influence of line width on $\mathbf{Z}_{\text{fringe}}$, however, is less clear. At a fixed detector length, the $\mathbf{Z}_{\text{fringe}}$ values would likely increase with decreasing width, though the quantitative dependence on the width is unknown. $\mathbf{Z}_{\text{fringe}}$ values will also be influenced by the thermal conductivity of the substrate and detector, \mathbf{Z}_{sub} , and \mathbf{Z}_d . Future studies should address these influences.

2.2.1 Responsivity

One key figure of merit to consider when designing and optimizing microbolometer performance is responsivity (\mathbf{r}), since the signal voltages can be quite low for these devices. A typical bismuth microbolometer has a responsivity of about 20 volts/watt, and noise equivalent power (NEP) on the order of 10^{-10} watts/ $\sqrt{\text{hertz}}$. The minimum detectable power will produce a signal in the nano-volt to micro-volt range for measurements taken in the 1-1000 Hz range. Detectors with higher responsivities could ease the amplification requirements in receiver systems by making it easier to detect these small signals. The thrust of the modeling presented here will be toward maximizing the responsivity of antenna-coupled microbolometers.

The signal voltage for a microbolometer can be related to the incident power by using a simple circuit expression for responsivity, given by

$$r = I_b \cdot \left(\frac{dR_D}{dP_L} \right) \left[\frac{\text{volts}}{\text{watt}} \right] \quad (2.14)$$

where I_b is the dc bias current through the detector, and $\frac{dR_D}{dP_L}$ is the change in resistance of the detector due power absorption in the load. For conventional bolometers, the load element also acts as the detector. The subscripts allow this expression to also describe composite microbolometer operation, where the load and the detector are separate elements.

According to equation 2.14, the responsivity can be optimized by maximizing the product of I_b and $\frac{dR_D}{dP_L}$. By breaking these terms into physical constants, the role of the material properties becomes much clearer. This relationship with physical properties is dependent on the limiting mechanism of operation. The maximum bias current, for instance, is likely to be limited by one of four things: 1) **Thermal Limits** of the detector due to I^2R (joule) heating, 2) **Current density limits** in order to avoid electromigration failure in the detector element, or due to the critical superconducting current density in superconducting materials; 3) **Bias-induced**

electric field breakdown across either the detector material or the dielectric between the detector and the load, or 4) **Instability** of the detector.

2.2.2 Thermally Limited Behavior

A microbolometer will experience heating due to the bias current as well as from incident power. By far, most of the power will come from the bias source across the detector. The maximum allowable temperature rise above ambient (ΔT_{\max})

$$\Delta T_{\max} = T_{\max} - T_{\text{amb}} \quad (2.15)$$

due to the maximum allowable dc bias power (P_{\max}) is

$$\Delta T_{\max} = P_{\max} \cdot Z_D \quad (2.16)$$

where Z_D is the thermal impedance of the detector, defined as

$$Z_D = \frac{dT_D}{dP_D} \quad (2.17)$$

Since the power dissipated in the detector is mostly due to joule heating from the bias source, ΔT_{\max} can be represented as

$$\Delta T_{\max} = I_{\max}^2 \cdot R_D \cdot Z_D \quad (2.18)$$

The maximum allowable detector bias current (I_{\max}), in terms of the maximum allowed temperature rise, is then

$$I_{\max} = \sqrt{\frac{\Delta T_{\max}}{R_D \cdot Z_D}} \quad (2.19)$$

The second term in equation 2.14 can be broken down into the following physical constants

$$\frac{dR_D}{dP_H} = R_D \cdot \alpha_D \cdot \eta_{th} \cdot Z_H \quad (2.20)$$

where α_D is the temperature coefficient of resistivity of the detector material

$$\alpha_D = \frac{1}{R_D} \cdot \frac{dR_D}{dT_D} \quad (2.21)$$

η_{th} is defined as the thermal coupling efficiency between the heater and the detector element

$$\eta_{th} = \frac{dT_D}{dT_H} \quad (2.22)$$

and Z_L is defined as the thermal impedance of the heater element

$$Z_L = \frac{dT_H}{dP_H} \quad (2.23)$$

For a conventional bolometer, $Z_L = Z_D$, and $\eta_{th} = 1$.

Substituting equations 2.19 and 2.20 into equation 2.14 reveals a new expression which relates to the physical constants to microbolometer responsivity for the thermally limited case.

$$r = \sqrt{\Delta T_{\max}} \cdot \sqrt{R_D} \cdot \alpha_D \cdot \left[\frac{\eta_{th} \cdot Z_H}{\sqrt{Z_D}} \right] \quad (2.24)$$

The bracketed terms are related, and cannot be varied independently. For convention bolometers, this relation can be reduced to

$$r = \sqrt{\Delta T_{\max}} \cdot \sqrt{R_D} \cdot \alpha_D \cdot \sqrt{Z_D} \quad (2.25)$$

The relations in equations 2.24 and 2.25 can be useful in evaluating the potential detector materials and configurations. The square root dependence on ΔT_{\max} shows that the responsivity may be improved by using detector materials that can withstand high temperatures. Materials which are resistant to oxidation and melting would make good candidates. Bismuth, because of its low melting point, is not capable of high temperature operation. ΔT_{\max} could also be increased by lowering the ambient temperature of the system. This is also likely to improve NEP by reducing the thermally-induced component of noise. However, the thermal conductivities of some materials, such as sapphire, increase with decreasing temperature, resulting in lowered thermal impedances. For composite structures, the dielectric layer must also be able to withstand operation at high temperatures. Because ΔT_{\max} has only a square root dependence, however, it is unlikely that this term alone would increase the responsivity by more than a factor of two.

The relations above also indicate that an improvement in responsivity would result from an increase in the thermal impedance of the detectors. It has been shown experimentally that preventing the detector from contacting the substrate by use of air-bridges increases the responsivity of a microbolometer by increasing the thermal impedance of the detector[4]. This method was reported to have increased responsivity by a factor of five, and the sensitivity was improved by a factor of four. Choosing detector materials to minimize thermal conductivity would also serve to increase thermal impedances. This criterion would tend to favor semiconductor or oxide materials over metallic detector materials. Choosing a high resistance detector may also be an easy way to increase responsivity. Even though this term has a square root dependence for the thermally limited case, it would be easy to find a detector material with a resistivity of many orders of magnitude higher than bismuth. For conventional microbolometers, the detector resistance is fixed in order to be impedance matched to the antenna. For composite structures, this restriction does not apply. The strong linear dependence of α_D on responsivity also makes this a key parameter in detector material choice.

2.2.3 Current Density Limited

Another mechanism which may limit responsivity by limiting the driving current through the detector may be device failure due to electromigration. The current density may also be limited in the case of superconducting microbolometers. In this case, it is assumed that the maximum allowable current is determined by the maximum allowable current density through the detector element, rather than a maximum allowable temperature rise. Although electromigration damage is generally dependent on temperature in most systems, this analysis will assume that the increase in temperature due to the bias current will be small and thus have a negligible effect on the maximum current density.

Equation 2.26 shows an expression for responsivity that is algebraically identical to equation 2.14.

$$r = I_b \cdot R \cdot \alpha \cdot Z \quad (2.26)$$

The maximum allowable current (I_{\max}) can be related to the maximum current density as

$$I_{\max} = J_{\max} \cdot t \cdot w \quad (2.27)$$

where t is the detector thickness, and w is the detector width. The detector resistance can be expressed as

$$R = \frac{\rho \cdot L}{t \cdot w} \quad (2.28)$$

where ρ is the resistivity of the detector material, and L is the physical length of the detector. Substitution of equations 2.27 and 2.28 into 2.26, where $I_b = I_{\max}$ results in the following expression for the dc voltage responsivity.

$$r = J \cdot \rho \cdot \alpha \cdot L \cdot Z \quad (2.29)$$

For the case of the air-bridge bolometer [4], the thermal impedance will be independent of the detector length (see section 2.1.2). For a given detector material, the length of the airbridge will determine the maximum responsivity of the device.

For moderately long substrate supported microbolometers, the thermal impedance is primarily determined by heat flow directly into the substrate. An empirical approximation for this case was presented in section 2.1.3, and is shown in equation 2.11. By using equation 2.11 to approximate Z , the responsivity can be expressed as

$$r = 1.2 \cdot \frac{J \cdot \rho \cdot \alpha}{k_{\text{sub}} \cdot \sqrt{2} \cdot \pi} \cdot \left(\frac{L}{w} \right)^{0.4} \quad (2.30)$$

This equation will over estimate the responsivity for short detector lengths due to the fringe mechanism of heat loss described in section 2.1.4.

These relations show that for bolometers in which bias current is limited by current density, there is a linear dependence on ρ as well as α . This criteria would favor bismuth over other metals as a detector material. Materials which are resistant to electromigration would also be favored for this case.

2.2.4 Thermal vs. Current Density

Experiments have shown that typical bismuth microbolometers with the following properties can be operated reliably for long periods of time at 2 milli-amps. The devices become unreliable at around 3 to 5 milli-amps.

length	width	thickness	resistance	responsivity	α
4 μm	2 μm	1500 \AA	$\sim 100 \Omega$	~ 20 volts/watt	$\sim 0.003 \text{ K}^{-1}$

Table 2.4 Operating parameters for a typical bismuth microbolometer

For the dimensions listed in table 2.1, the current density at 0.003 amps would be 10^6 amps/cm², which suggests the possibility that failure may be due to electromigration damage.

The temperature rise due to the bias current can be approximated by using

$$\Delta T = \frac{r \cdot I_b}{\alpha} \quad (2.31)$$

This estimates a 20 °C temperature rise above ambient ($\sim 300 \text{ K}$) when biased at about 0.003 amps. This temperature of $\sim 45 \text{ }^\circ\text{C}$ is much lower than the melting point of bismuth (544 °C), which makes it unlikely that failure is due to melting of the bismuth element. Failure due to oxidation is also unlikely if these temperatures are accurate.

Though the observations shown here are not entirely conclusive, they do suggest that electromigration is the most likely mechanism for limiting current in bismuth microbolometers.

2.2.5 Electric Field Breakdown

Composite microbolometers have an extra vulnerability that does not exist with conventional microbolometers, in that voltage differences between the heater and the detector element will result in high electric fields within the dielectric that separates the two elements. The likelihood of accidentally stressing the dielectric may be reduced by grounding one lead of the antenna to one of the detector leads. The dielectric will also experience electric fields due to the detector bias voltage. The electric circuit for electric fields induced by the bias voltage is illustrated in figure 2.9. The highest fields will be at E_1 , where they will be roughly

$$E_{\max} \approx \frac{V_D}{2 \cdot t_{\text{die}}} \quad (2.32)$$

where V_D is the detector bias voltage, and t_{die} is the thickness of the dielectric material that separates the heater from the detector.

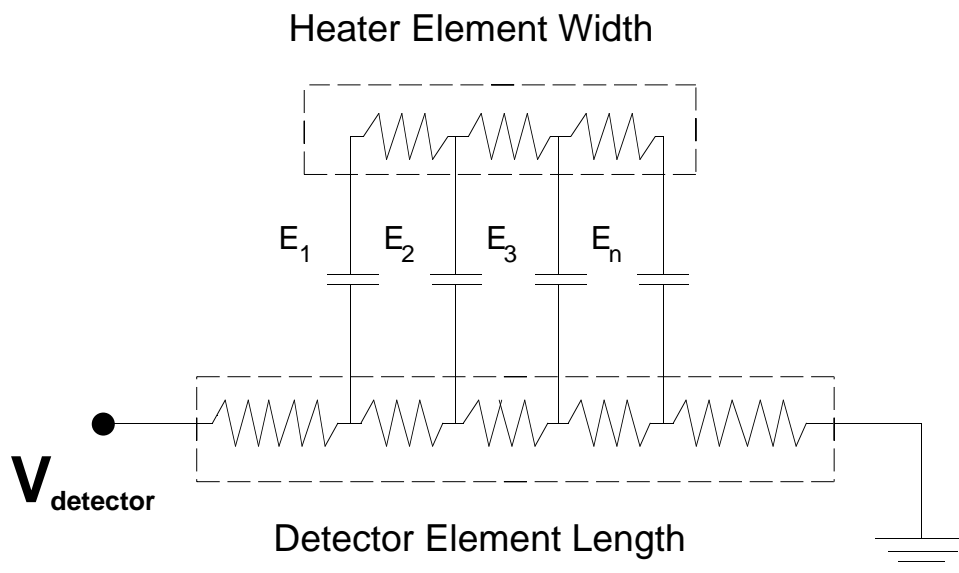


Figure 2.9 Electrical circuit for a composite microbolometer showing the distribution of electric field within the dielectric.

If electric field-induced breakdown is the limiting factor, then the maximum responsivity can be given as

$$r = V_{\text{BD}} \cdot \alpha_{\text{D}} \cdot \eta_{\text{th}} \cdot Z_{\text{th}} \quad (2.33)$$

where V_{BD} is the breakdown voltage of the device.

This behavior would be more likely for high resistance detectors where high bias voltages (> 10 V) could be used without dissipating much power. For a dielectric thickness of 1000 \AA , only 10 volts would be needed to produce an electric field of 10^6 V/cm, which is about the breakdown field of a good physically-deposited dielectric material. The electric field through the dielectric could be reduced by using a thicker dielectric, but at the expense of lowering the thermal coupling coefficient (η_{h}). Leakage currents through a stressed dielectric may also contribute significantly to signal noise.

2.2.6 Microbolometer Stability

Another issue which affects microbolometer operation and can limit responsivity is stability under constant bias conditions. Using a higher bias across the detector will generally increase responsivity and thus will result in a larger signal. A linear relationship between bias current and responsivity is described in equation 2.14. and implies that it will be linear as long as the other parameters (dR/dT , α , k) remain independent of bias current.

It is important to remember that there are two components of power that are dissipated in the detector. The incident radiation received from the antenna is one component dissipated in the detector, and will be considered an independent variable for this analysis. The other component is power dissipated from the bias current, which will normally be much higher than the incident power. The key point is that incident power (P_{incident}) can influence the bias power (P_{b}) by changing the detector resistance. This will result in either positive or negative feedback, depending on whether the device is biased at constant current or constant voltage, and whether the detector has a positive or negative temperature coefficient of resistance.

Table 2.5 shows the conditions which result in positive or negative feedback.

Bias typeTemp.	Coeff. of Resistance	Type of Feedback
constant current	$\alpha > 0$	positive
constant current	$\alpha < 0$	negative
constant voltage	$\alpha > 0$	negative
constant voltage	$\alpha < 0$	positive

Table 2.5 Feedback bias relationships

For example, under constant current bias and a positive coefficient of resistance ($\alpha > 0$), incident power will increase the resistance of the detector. Since the bias

current is held constant, this will increase the bias power, thus further increasing the resistance and further increasing the bias power.

Experience has shown that some operating conditions can result in unstable positive feedback where runaway current destroys the device. I have seen instabilities even in large area (100 μm x 1000 μm) superconducting Bi-Sr-Ca-Cu-O bolometers[5] when operated at high currents, although these devices were large enough to dissipate a 10 volt bias without destroying themselves. Superconducting devices could be voltage biased in order to avoid positive feedback; however, destructively high currents could occur if the device temperature drifts too close to the superconducting state. In these cases, the maximum bias conditions are lower than what would be predicted when positive feedback effects are ignored. In order to better understand and predict the maximum stable bias, an analysis is given here.

The following definitions will be used for this discussion:

$$r = \text{small signal responsivity} = I_b \cdot \frac{dR}{dP} = I_b \cdot \frac{dR}{dT} \cdot Z \quad [V/W]$$

$$I_b = \text{bias current [I]}$$

$$Z = \text{Thermal Impedance} = \frac{dT}{dP} \left[\frac{^\circ C}{W} \right]$$

$$\Delta V_n = \text{Incremental feedback voltage across detector calculated at } n^{\text{th}} \text{ iteration.}$$

$$P_o = \text{Instantaneous Power at time} = 0. \text{ (Bias + Incident. Does not include feedback)}$$

$$\Delta P_n = \text{Feedback power calculated at } n^{\text{th}} \text{ iteration.}$$

From the above definitions, ΔV_1 , the initial voltage change across the detector due to the bias power and the incident power, can be expressed as:

$$\Delta V_1 = r \cdot P_o \quad (2.34)$$

The incremental increase in power dissipated in the detector (joule heating) caused by the increased bias voltage can be expressed as:

$$\Delta P_1 = \Delta V_1 \cdot I_b = r \cdot P_o \cdot I_b \quad (2.35)$$

This increase in power in the detector then causes another incremental increase in detector voltage that can be expressed as:

$$\Delta V_2 = r \cdot \Delta P_1 = r \cdot P_0 \cdot [r \cdot I_b] \quad (2.36)$$

Further iterations of the incremental increases in bias voltage due to feedback can be expressed as:

$$\Delta V_n = r \cdot P_0 \cdot [r \cdot I_b]^{n-1} \quad (2.37)$$

The total increase in detector voltage due to feedback can then be expressed as:

$$\Delta V_{\text{Feedback}} = r \cdot P_0 \cdot \sum_{m=0}^{\infty} (r \cdot I_b)^m \quad (2.38)$$

By using the following relation:

$$\sum_{z=0}^{\infty} A^z = \frac{1}{1-A} \quad \text{for } (A < 1) \quad (2.39)$$

the total feedback voltage can then be expressed as

$$V_{\text{Feedback}} = \frac{r \cdot P_0}{1 - r \cdot I_b} \quad (2.40)$$

From this relation it is apparent that the following must be true for stable operation:

$$r \cdot I_b < 1 \quad (\text{For stable operation}) \quad (2.41)$$

Another form of this relation looks like:

$$I_b^2 \cdot \frac{dR}{dT} < \frac{1}{Z} \quad (2.42)$$

These results suggests that high resistance detectors would be more stable than low resistance detectors. This criterion should be considered when modeling low resistance detectors, such as superconducting microbolometers. However, if high resistance detectors are integrated with a composite microbolometer structure, operation may be limited by electric field breakdown in the dielectric between the heater and the detector.

References

1. D. P. Neikirk, W. W. Lam, and D. B. Rutledge, "Far-Infrared Microbolometer Detectors," *International Journal of Infrared and Millimeter Waves*, **5**, 245 - 278 (3 1984).
2. S. M. Wentworth, "Far-Infrared Microbolometer Detectors", Doctoral Dissertation, University of Texas at Austin, 1990
3. V. M. Abrosimov, B. N. Ergorov, and M. A. Krykin, "Size Effect of Kinetic Coefficients in Poly Crystalline Bismuth Films," *Sov. Phys. JETP*, **37**, 113-116 (1 1973).
4. D. P. Neikirk, and D. B. Rutledge, "Air-bridge Microbolometer for Far-infrared Detection," *Applied Physics Letters*, **44**, 153-155 (15 January 1984).
5. J. M. Lewis, "Optical Detectors Based on Superconducting Bi-Sr-Ca-Cu-Oxide Thin Films", Undergraduate Thesis, Massachusetts Institute of Technology, 1989